

POST-COMMON-ENVELOPE BINARY STARS AND THE PRECATAclysmic BINARY PG 1114+187

TODD C. HILLWIG,¹ R. KENT HONEYCUTT,¹ AND JEFF W. ROBERTSON²

Received 2000 March 27; accepted 2000 April 25

ABSTRACT

We present orbit-resolved spectroscopy and orbit-sampled photometry of the binary system PG 1114+187. Both photometry and radial velocity studies reveal a period $P = 1.75992$ days, which is taken to be the orbital period of the binary. Strong modulation of emission-line strength with the same period is also present. A preliminary mass ratio, $M_2/M_1 \approx 0.7$, is found from primary- and secondary-star radial velocity amplitudes. No evidence is seen for either an accretion disk or mass transfer, leading to the conclusion that PG 1114+187 is not a cataclysmic variable (CV) but is in a pre-CV state, before the initiation of mass transfer. The short orbital period also leads to the conclusion that the system passed through a common-envelope phase at some time in the past. The current list of known post-common-envelope and precataclysmic binary stars is also reviewed and the general properties of this class of star are discussed.

Key words: binaries: close — stars: individual (PG 1114+187)

1. INTRODUCTION

PG 1114+187 is a poorly studied variable found in the Palomar-Green survey (Green, Schmidt, & Liebert 1986) that has received preliminary classification as a cataclysmic variable (CV; Downes & Shara 1993; Downes, Webbink, & Shara 1997) but has never had conclusive evidence presented to that end. Initial observations of its *UBV* color (Bruch & Engel 1994) and spectrum (Zwitter & Munari 1994) were not inconsistent with those of typical CVs. However, further photometric study (Misselt & Shafter 1995), although preliminary, showed no signs of the flickering common to CV systems.

Photometry and orbit-resolved spectroscopy presented here lead to the removal of the classification of PG 1114+187 as a CV and to its classification as a post-common-envelope binary (PCEB) and precataclysmic binary (PCB). In addition, an orbital period obtained through photometry, radial velocity studies, and emission-line modulations is presented.

2. POST-COMMON-ENVELOPE BINARIES

The first PCEBs were discovered as eclipsing binary systems (for recent studies see Ibanoglu et al. 1994, for V471 Tau; Ferguson et al. 1999, for BE UMa) typically containing a low-mass main-sequence star and a hot compact companion. The primaries are generally white dwarf or subdwarf stars that have progressed through stages of envelope expansion and ejection. The orbital periods of these stars, typically on the order of a few days or less (see Table 1), reveal that an expanded envelope on the order of 1 AU would have easily encompassed the low-mass companion. This would create a common-envelope configuration.

Not all PCEBs are PCBs, however. Most CVs contain a white dwarf primary and a red dwarf secondary star. Some PCEBs have white dwarfs with upper main-sequence or even white dwarf or subdwarf companions. In addition, the processes that reduce the orbital periods of these systems

(thought to be gravitational radiation and magnetic braking) act very slowly. We can find the time for each system to become semidetached because of gravitational radiation from Warner (1995) by using

$$t_{sd} = 4.73 \times 10^{10} \frac{(1+q)^{1/3}}{q} M_1^{-8/3}(1) \times [P_i^{8/3}(d) - P_f^{8/3}(d)]y, \quad (1)$$

where q is the ratio of the mass of the secondary to the mass of the primary, $M_1(1)$ (using Warner's notation) is the mass of the primary in units of solar mass, P_i is the current orbital period, and P_f is the orbital period at contact, found by using

$$P_f(d) = 0.37M_1^{4/5}(2) \text{ for } P_f(d) \lesssim 0.38. \quad (2)$$

Using this formulation, most systems for which we can calculate the time until contact have t_{sd} greater than a Hubble time. Magnetic braking, if present, would likely dominate over gravitational radiation for orbital periods $\gtrsim 2.0$ hr. It is possible, however, that for systems with $M_2 \lesssim 0.25 M_\odot$, where the secondary is fully convective, complicated field lines prevent or limit a stellar wind (Taam & Spruit 1989). Because of the many unknowns in magnetic braking, the quantitative contribution it produces is less certain. Warner (1995) provides an approximate equation analogous to equation (1),

$$t_{sd} \approx \frac{8.26 \times 10^6}{(1+q)^{1/3} q^{2/3} M_1^{2/15}(2) [k^2(2)/0.1]} \times \left[\left(\frac{P_i}{P_f} \right)^{10/3} - 1 \right] y, \quad (3)$$

where $k(2)$ is the radius of gyration of the portion of the secondary that is coupled to the wind. Even considering this mechanism, most current PCEBs have values of $t_{sd} \gtrsim t_H$, the Hubble time. This, of course, leads to the question of whether current CVs passed through a detached, PCB state or evolved directly into contact during the common-envelope phase. This question has been discussed extensively in the literature and is beyond the scope of this paper.

In addition to eclipses, PCEBs have also been discovered through studies of photometric and spectral variations

¹ Department of Astronomy, Swain Hall West 319, Indiana University, Bloomington, IN 47405; thillwig@astro.indiana.edu, honey@astro.indiana.edu.

² Department of Physical Sciences, Arkansas Tech University, Russellville, AR 72801-2222; Jeff.Robertson@mail.atu.edu.

TABLE 1
PROBABLE POST-COMMON-ENVELOPE BINARIES WITH $P_{\text{orb}} < 16$ DAYS

Star	R.A. (hr)	Decl. (deg)	V^a	P (hr) ^b	$M_1(1)$	$M_1(2)$	T (K)	i (deg)	Comment ^c	Refs.
Feige 24	03	+04	12.40	4.23160d	0.47 ± 0.03	0.295 ± 0.035	Irr	1
V664 Cas	03	+65	13.38	13.96	Irr, PNN	2
CC Cet	03	+10	15.23	6.823	0.40 ± 0.11	0.18 ± 0.05	Irr	3, 4
BPM 71214	03	-09	14.2b	4.33	?	5
V471 Tau	04	+17	9.2	12.508	0.76 ± 0.02	0.73 ± 0.03	32,400	...	Ecl, Irr	6, 7
RR Cae	04	-49	14.36	7.289	0.467	0.095	7,000	84.0 ± 0.2	Ecl, rv	8
HZ 9	05	+18	13.93	13.544	0.51 ± 0.10	0.28 ± 0.04	22,000	...	rv, accr?	9
HD 33959C	05	+33	7.95	90.96	1.0:	1.8	rv, quadruple	10
AA Dor	06	-70	11.20	6.277	0.25 ± 0.05	0.043 ± 0.005	40,000	...	Ecl	11, 12
HD 49798	07	-44	8.30	37.1441	1.75 ± 1.0	1.75:	X-ray pulsator, rv	13, 14
V651 Mon	07	-01	10.8b	15.991d	0.40 ± 0.05	1.8 ± 0.3	100,000	...	PNN, Irr?	15
GD 448	07	+74	14.97	2.473	0.41 ± 0.01	$0.096 \pm .004$	Irr	16, 17
IN CMa	07	-32	16.1	24.5	0.49-0.62	0.49-0.79	52,400	...	Irr	18, 19
VW Pyx	09	-29	16.5	16.09	PNN, ?	20
BI Lyn	09	+40	12.87	8.116	Irr	21, 22
RE 1016-053	10	-05	14.3	18.943	0.61 ± 0.1	0.16	55,400	...	Irr	23, 24, 25
PG 1026+002	10	-00	13.8	14.334	0.68 ± 0.23	0.22 ± 0.05	Irr	3, 26
KV Vel	11	-49	11.78	8.571	0.55 ± 0.15	0.25 ± 0.06	Irr, PNN	27
Feige 36	11	+25	12.78	4.94	0.5:	> 0.42	rv, WD pair	28
PG 1114+187	11	+18	14.6b	42.2369	Irr	This paper
BE UMa	12	+49	14.8	54.988	0.70 ± 0.07	0.36 ± 0.07	105,000	$84. \pm 1.$	Ecl, Irr, PNN	29
TW Crv	12	-19	12.77	7.86	Irr	30
UX CVn	12	+37	13.10	13.769	0.39 ± 0.05	0.42	28,000	90.	Ecl	31, 32
EG UMa	12	+53	13.34	16.023	0.38 ± 0.07	0.26 ± 0.04	13,000	...	rv, accr?	9
PG 1224+309	12	+31	16.16	6.2085	0.45 ± 0.05	0.28 ± 0.05	29,300	...	Irr	33
HW Vir	13	-09	9.4	2.801	0.54 ± 0.09	0.16 ± 0.03	36,500	81.6 ± 0.5	Ecl	34
EC 13471-1258	14	-13	14.80	3.617	?	35
SuWt 2	14	-59	12.29	58.8	Ecl, PNN	36
GK Vir	14	+01	17.0b	8.264	0.51 ± 0.04	0.10	Ecl, Irr	37
PG 1538+269	16	+27	13.83	60.02	0.5:	> 0.68	25,200	...	rv, WD pair?	38
SP 1	16	-52	13.9	69.8	Irr, PNN	39
NN Ser	16	+13	16.6	3.122	0.54 ± 0.07	0.12 ± 0.03	Irr	40, 41
HaTr 4	17	-51	17.1	41.0	Irr, PNN	39
G 203-47	17	+44	11.77	14.7136	0.5:	> 0.2 (M3.5)	rv	42
MT Ser	17	-15	15.95	2.717	0.6:	0.2 ± 0.1	50,000	...	Irr, PNN	43, 44
V477 Lyr	19	+27	15.07	11.321	0.51 ± 0.07	0.15 ± 0.02	Ecl, Irr, PNN	45
Hf 2-2	19	-29	...	9.566	Irr, PNN	46
UU Sge	20	+17	14.67	11.162	0.63 ± 0.06	0.29 ± 0.03	87,000	...	Ecl, PNN	47
Abell 65	20	-23	15.90	24.00	80,000	...	Irr, PNN	39, 48
RE 2013+400	20	+40	14.6	16.932	0.57 ± 0.1	0.19	48,000	...	Irr	23, 25, 49
FF Aqr	22	-03	9.31	9.2078d	0.5	2.0	...	81.	Ecl, Irr	50
MS Peg	23	+25	13.68	4.168	0.48 ± 0.02	0.22 ± 0.02	22,170	...	Irr	51

^a Items followed by *b* are *B* magnitudes.

^b Those periods followed by *d* are given in days.

^c Denotes method of determination of binarity: (Ecl) eclipses; (Irr) irradiation effect (equivalent width or photometric variations); *r(v)* radial velocity studies; (accr) possible mass transfer due to a wind or transient accretion stream; (?) literature is unclear. For other comments, see text.

REFERENCES.—(1) Vennes & Thorstensen 1994; (2) Grauer et al. 1987; (3) Saffer et al. 1993; (4) Somers et al. 1996; (5) Livio & Shara 1987; (6) Barstow et al. 1997; (7) Ibanoglu et al. 1994; (8) Bruch 1999; (9) Stauffer 1987; (10) Tokovinin 1997; (11) Sarna 1985; (12) Kudritzki et al. 1982; (13) Kudritzki & Simon 1978; (14) Israel et al. 1997; (15) Mendez et al. 1985; (16) Marsh & Duck 1996; (17) Maxted et al. 1998; (18) Barstow et al. 1995b; (19) Vennes & Thorstensen 1996; (20) Bond & Grauer 1987; (21) Lipunova & Shugarov 1991; (22) Orosz, Wade, & Harlow 1997; (23) Wood, Harmer, & Lockley; (24) Thorstensen, Vennes, & Bowyer 1996; (25) Vennes, Thorstensen, & Polomski 1999; (26) Bruch & Diaz 1999; (27) Landolt & Drilling 1986; (28) Moran et al. 1999; (29) Ferguson et al. 1999; (30) Chen et al. 1995; (31) Schönberner 1978; (32) Greenstein 1973; (33) Orosz et al. 1999; (34) Wood & Saffer 1999; (35) Warner 1995; (36) Bond 2000; Tylenda et al. 1991; (37) Fulbright et al. 1993; (38) Saffer et al. 1998; (39) Bond & Livio 1990; (40) Wood & Marsh 1991; (41) Catalán et al. 1994; (42) Delfosse et al. 1999; (43) Grauer & Bond 1984; (44) Green, Liebert, & Wesemael 1984; (45) Pollacco & Bell 1994; (46) Lutz et al. 1998; (47) Bell, Pollacco, & Hildich 1994; (48) Walsh & Walton 1996; (49) Barstow et al. 1995a; (50) Marilli et al. 1995; (51) Schmidt et al. 1995.

caused by the irradiated hemisphere of the low-mass secondary. For young PCEB systems or those with very hot primaries, UV radiation striking the interior hemisphere of the secondary star is reprocessed and emitted primarily in the optical part of the spectrum (Ferguson & James 1994). This creates a photometric variation as the heated hemisphere is alternately hidden and presented face-on to the observer as the system rotates.

When the irradiated hemisphere is visible, emission lines from radiation reprocessed in the outer layers of the secondary typically dominate the absorption spectrum of the subdwarf or white dwarf primary. The appearance of these emission lines led to the misclassification of some of these systems as CVs. However, the emission lines produced in PCEBs are much narrower than most CV emission lines, which are broadened by the rotation of an accretion disk.

The broadening mechanisms in PCEBs are rotation of the secondary and thermal broadening. In addition, if the system is at an inclination that causes variations in the visible surface area of the irradiated hemisphere (all but those with inclinations near zero), the emission lines show corresponding changes in equivalent width.

This situation leads to very specific phase relations among radial velocities, photometry, and emission-line strengths. We denote the primary star as the hotter star, or star 1. Superior conjunction of the primary (primary eclipse for an eclipsing system) is taken as orbital phase $\phi = 0.0$. The system appears brightest at superior conjunction of the secondary when the irradiated hemisphere is facing the observer, or $\phi = 0.5$. At this point the radial velocity of the secondary is changing from positive to negative through zero and the emission-line strength is expected to be greatest.

Table 1 provides a list of probable PCEBs that have been detected by the methods described above. Masses are given in M_{\odot} and temperatures listed are for the primary star. The remaining columns are self-explanatory. Approximate coordinates are given as indicators of seasonal and latitudinal observability. A few additional systems that were discovered by means of radial velocity variations but that do not show eclipses or irradiation effects have also been included. These may be systems consisting of a hot subdwarf and upper main-sequence star or those with an old, low-temperature subdwarf incapable of heating the secondary to a significant degree for reprocessing to be observable. We do not include systems with orbital periods longer than that of V651 Mon (15.991 days), for which certainly $t_{sd} \gg t_H$ even when considering both gravitational and magnetic braking. Systems not confirmed as close binaries or discovered to be close but with no reported orbital period are not listed.

Several objects in Table 1 have additional characteristics noted in the comments column. Thirteen are known planetary nebula nuclei (PNNs), and brief descriptions of four other systems follow.

HD 33959C: This is a quadruple system containing two close binary systems (Tokovinin 1997). One is an F3V-M3V pair with an orbital period of 2.99 days. The other is an A9 IV-WD pair with an orbital period of 3.79 days. The white dwarf identification is uncertain.

HD 49798: This is an X-ray pulsator (Israel et al. 1997) that is seen to have periodic radial velocity variations with $P = 37.1441$ hr. The primary is an sdO star and the companion is another degenerate, quite possibly a neutron star.

Feige 36, PG 1538+269: These were discovered as binary systems via strong radial velocity variations. The masses are not well known, but it is believed that both systems are white dwarf pairs (for Feige 36, see Moran et al. 1999; for PG 1538+269, see Saffer, Livio, & Yungelson 1998).

3. OBSERVATIONS AND REDUCTIONS OF PG 1114+187

3.1. Photometry

The photometric data consist of V-band CCD photometry obtained during the interval October 1993 to May 1999 with the Indiana Automated CCD Photometric Telescope, also known as RoboScope (Honeycutt et al. 1990; Honeycutt & Turner 1992). A total of 260 usable 4 minute exposures were reduced by inhomogeneous ensemble pho-

tometry (Honeycutt 1992) using 17 comparison stars. The errors range from ~ 0.005 to ~ 0.015 mag. The zero point is determined using four secondary standard stars from Henden & Honeycutt (1997) and has an uncertainty of 0.02 mag. The 6 yr light curve for PG 1114+187 displayed in Figure 1 shows short-term variations of 0.13 mag and no long-term trends.

The periodogram in Figure 2 was produced using the period search technique of Scargle (1982) as modified by Horne & Baliunas (1986). The three major peaks corre-

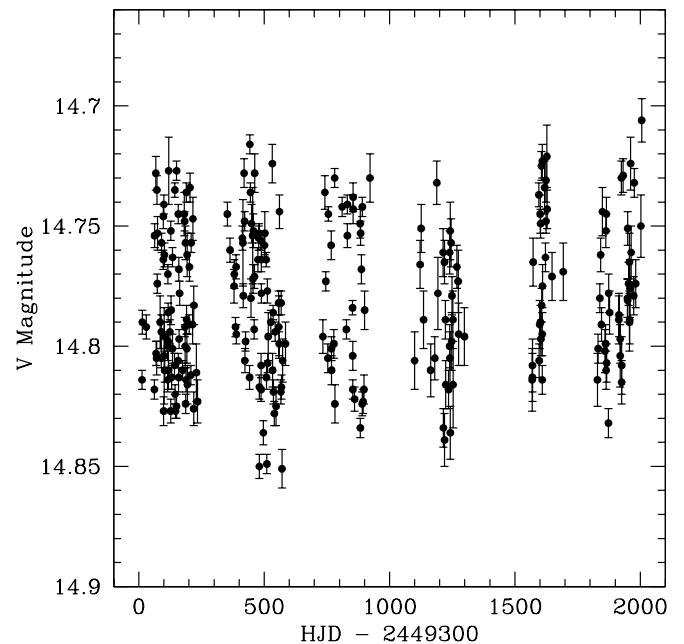


FIG. 1.—Light curve for PG 1114+187 covering the interval October 1993 to May 1999.

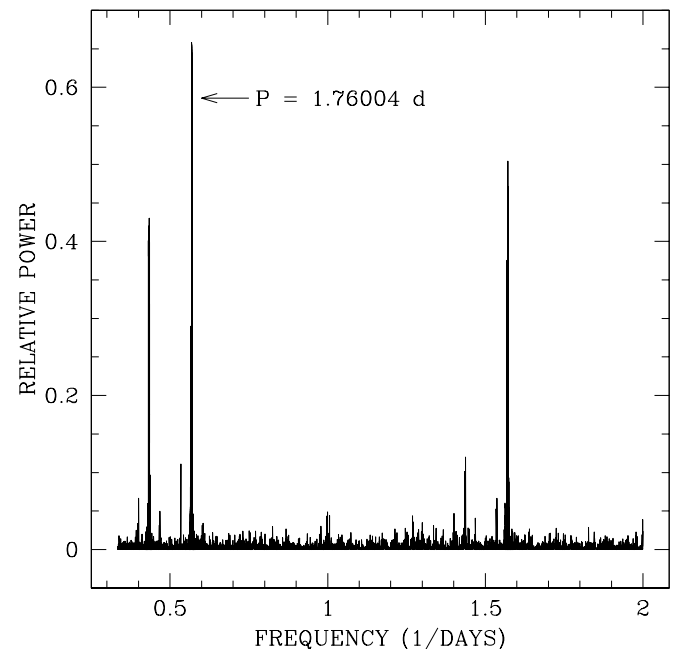


FIG. 2.—Periodogram for the light curve in Fig. 1. The labeled peak is believed to represent the true orbital period, accompanied by two alias peaks.

TABLE 2
PHOTOMETRIC SINE WAVE FITTED
PARAMETERS

Parameter	Value
V_{mean}	14.7827 ± 0.0004
Amplitude.....	0.0373 ± 0.0005
T_0	2449312.586 ± 0.004
P	1.75992 ± 0.00003

spond to 2.31607, 1.70064, and 0.63653 days. Folding the data on these three periods yields rms values from a sine wave of 0.0240, 0.0179, and 0.0221 respectively. The peak at period $P = 1.76004$ days has both the greatest power in the periodogram and the lowest rms deviation from a sine wave. Visual inspection of the folded light curves also greatly favors this period, as do rms deviations for the spectroscopic data discussed in the following section. We take this approximate period as a starting point for fitting a sine curve of the form

$$V_{\text{mean}} = V + K \sin [(2\pi/P)(T - T_0) + \phi], \quad (4)$$

where V is the visual magnitude, K is the amplitude, and P is the period; either T_0 or ϕ is a fitted parameter. For the photometry we set $\phi = 0.75$ and fit for T_0 and the remaining parameters, anticipating this phase shift from the spectroscopic data, whose behavior defines the orbital phasing. The derived photometric ephemeris for minimum light is

$$T = (2449312.586 \pm 0.004) + (1.75992 \pm 0.00003)E, \quad (5)$$

and the fitted parameters are listed in Table 2. Figure 3 shows the light curve folded on this ephemeris and the sine curve fit. The rms variation of the data from the fitted sine curve is 0.0174 mag. Such a small scatter rules out flickering from an accretion disk commonly seen in CVs.

3.2. Spectroscopy

A total of 44 spectra of PG 1114+187 were obtained on 1998 March 8–11 with the WIYN multiobject

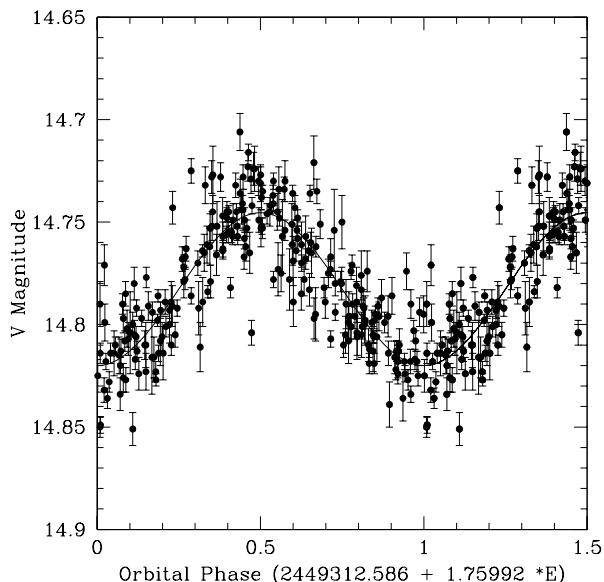


FIG. 3.—Phase-folded light curve of PG 1114+187 for the given ephemeris.

TABLE 3
IDENTIFIED EMISSION LINES

λ (Å)	I.D.	EW (Å)	$F_x/F_{H\beta}$
6676.596.....	He I 6678.1	−1.66	0.472
6560.280.....	H α	−7.92	2.25
5874.217.....	He I 5875.6	−2.11	0.599
5167.211.....	Fe I 5167.5 ?	−0.65	0.18
5015.168.....	He I 5015.7	−1.07	0.304
4920.260.....	He I 4921.9	−0.74	0.21
4860.096.....	H β	−3.52	1.00
4713.704.....	He I 4713.1 \pm 0.4	−0.32	0.09
4470.466.....	He I 4471.7	−0.50	0.14
4339.235.....	H γ	−2.07	0.588
4100.805.....	H δ	−2.16	0.614

spectrograph³ using the Hydra fiber positioner (March 8) and the DensePak fiber array (March 9–11), both with the Bench spectrograph camera. A 600 line mm^{−1} grating with a 13°9 blaze angle was used. The central wavelength was 5300 Å, covering the range 3885–6731 Å with 3 Å resolution.

Hydrogen Balmer and He I lines were seen in emission. For a listing of identified emission lines and their relative strengths (at $\phi = 0.5$, or maximum light) see Table 3.

3.2.1. Emission-Line Radial Velocities

Radial velocities of the H α , He I 6678 Å, and He I 5876 Å lines were measured. Line centers were found using a best-fit Gaussian profile of variable width and height, and the radial velocities were converted to the heliocentric frame. The resulting data are displayed in Table 4. The strength of the H α emission line permitted its measurement at all phases. The He I lines, however, disappeared into the continuum noise near $\phi = 0$. Fewer measurements were obtained for He I 6678 Å than for He I 5876 Å because of the lower signal-to-noise ratio (S/N) in that line. Additionally, contamination of He I 5876 emission by the nearby NaD absorption line was present in all spectra. Measurements that were overly contaminated were discarded.

Periodograms of the radial velocity data for each line were inconclusive. However, constraining the period to the photometric period produces the results in Figure 4. In this case, in equation (4), V and V_{mean} are now radial velocities, T_0 is set from the photometric ephemeris, and ϕ is a fitted parameter. The parameters of the H α and He I fits generally agree with one another to within respective errors. There is a phase difference of ≈ 0.1 between the H α and He I fits, however. This is possibly because of the NaD absorption lines at 5891 Å contaminating the He I emission line and skewing the line center measurements. Both fits also yield phase shifts from photometry of $\phi(rv) - \phi(\text{phot}) \approx 0.25$, as expected.

3.2.2. Emission-Line Equivalent Width

Also apparent in the spectra is an orbital modulation of the equivalent widths of the emission lines, particularly the H α line. Figure 5 shows representative spectra by orbital

³ The WIYN Observatory is jointly operated by the University of Wisconsin, Indiana University, Yale University, and the National Optical Astronomy Observatories.

TABLE 4
H α AND HE I EMISSION-LINE RADIAL VELOCITIES

HJD	V_{rad} (km s $^{-1}$)		
	H α	He I 5876	He I 6678
2,450,880.83164.....	51.
2,450,880.84227.....	45.
2,450,880.86063.....	44.
2,450,880.87771.....	54.
2,450,881.68274.....	-120.	-73.	-71.
2,450,881.69956.....	-126.	-70.	-80.
2,450,881.71487.....	-128.	-70.	-72.
2,450,881.73018.....	-133.	-80.	-83.
2,450,881.74578.....	-135.	-86.	-94.
2,450,881.76109.....	-139.	-81.	-95.
2,450,881.77639.....	-144.	-93.	-95.
2,450,881.79339.....	-146.	-92.	-110.
2,450,881.80870.....	-147.	-86.	-104.
2,450,881.82401.....	-149.	-100.	-99.
2,450,881.84186.....	-155.	-105.	-133.
2,450,881.85717.....	-153.	-106.	-132.
2,450,881.87248.....	-156.	-99.	-94.
2,450,882.74284.....	62.	44.	23.
2,450,882.75816.....	60.	51.	66.
2,450,882.77347.....	63.	39.	88.
2,450,882.78906.....	56.	59.	86.
2,450,882.80437.....	59.	53.	55.
2,450,882.81968.....	61.	50.	91.
2,450,882.83937.....	69.	65.	59.
2,450,882.85468.....	69.	39.	43.
2,450,882.87000.....	61.	43.	78.
2,450,882.88571.....	61.	59.	106.
2,450,882.90103.....	65.	46.	88.
2,450,882.91634.....	64.	56.	91.
2,450,882.93282.....	68.	63.	68.
2,450,882.94813.....	65.	54.	68.
2,450,883.71950.....	-112.	-136.	-103.
2,450,883.73481.....	-114.	-140.	-96.
2,450,883.75013.....	-120.	-156.	-110.
2,450,883.76888.....	-122.	-114.	-88.
2,450,883.78419.....	-114.	-154.	-116.
2,450,883.79950.....	-117.
2,450,883.81500.....	-115.	-139.	...
2,450,883.83031.....	-119.
2,450,883.84562.....	-111.	-145.	...
2,450,883.86407.....	-129.
2,450,883.87938.....	-125.
2,450,883.92261.....	-126.
2,450,883.93792.....	-106.

phase. Plotting the equivalent widths of the H α line constrained to the photometric orbital period results in the phase-folded plot in Figure 6. The sine fit to this data, using our derived ephemeris, yields the expected phase shift from the photometric and radial velocity curves (i.e., EW maximum occurs at photometric maximum).

3.2.3. Absorption-Line Radial Velocities

Broad Balmer absorption lines are very noticeable in the spectra near $\phi = 0.0$ (see the H β region of the $\phi = 0.1$ spectrum, upper left of Fig. 5). The profile of these lines (very broad shallow wings) suggest that they originate from the white dwarf. In fact, similar absorption lines have been observed in many other PCEBs. Accurate measurement of the radial velocity curves of these lines can produce a measurement of the mass ratio, $q = M_2/M_1$, since we have

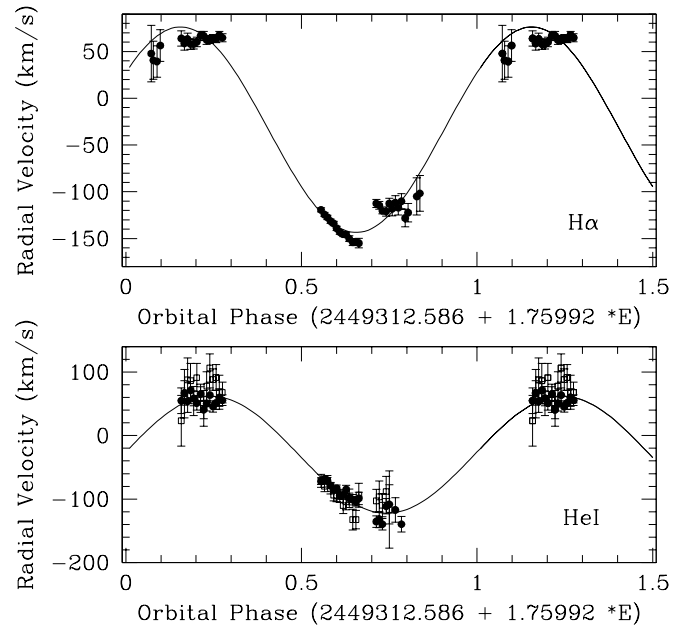


FIG. 4.—Radial velocity curves for the H α and He I 5876, 6678 Å lines, constrained to the photometric period.

determined the radial velocity amplitude of the secondary star.

The absorption lines grow in strength relative to the secondary's emission lines as the order of the Balmer line increases. Therefore the H β absorption line is more easily visible near maximum brightness than is the H α absorption line. The S/N is very degraded near the H γ line and at shorter wavelengths, requiring that the H β absorption line be used. Attempts were made at measuring both the H γ and

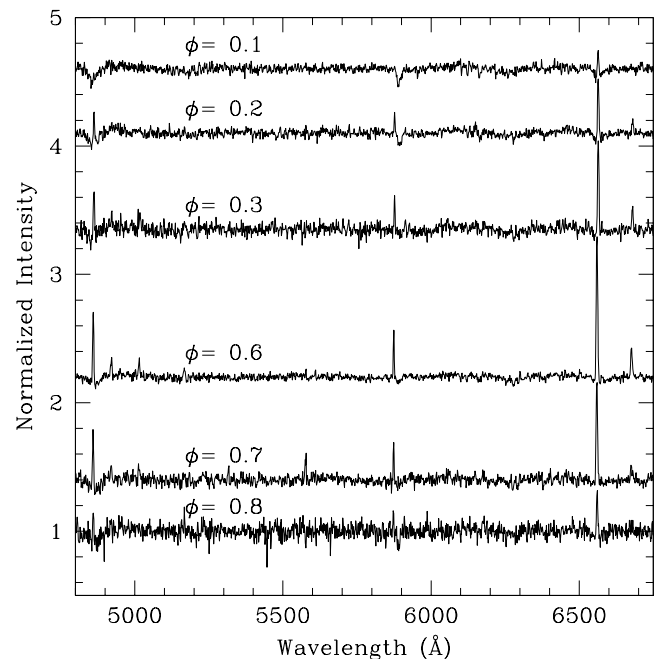


FIG. 5.—Representative spectra arranged by photometric orbital phase showing modulation of the emission-line strengths.

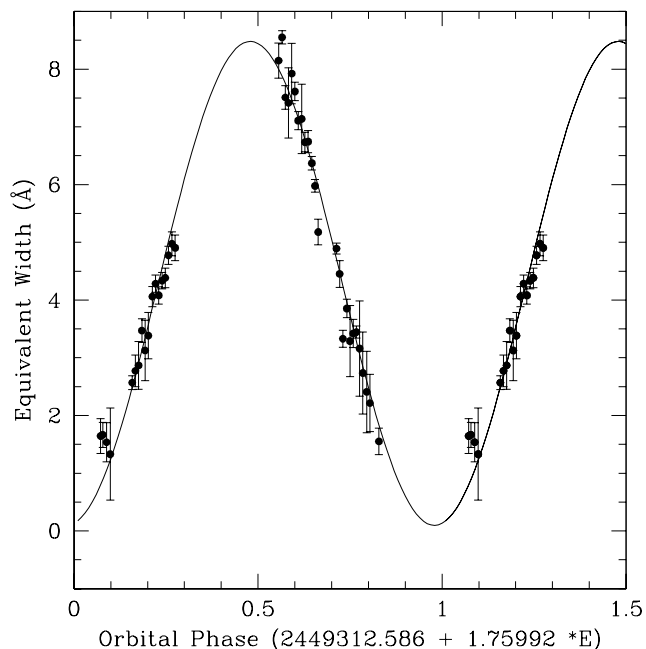


FIG. 6.—Equivalent widths of the $H\alpha$ line constrained to the photometric period.

$H\alpha$ lines, but they were dominated, respectively, by noise and emission from the secondary to such a degree that reliable data could not be obtained.

To increase the signal-to-noise ratio, consecutive spectra were coadded into bins of ≈ 1 hr, or 0.025 phase units. To obtain line center, the continuum and absorption line were fitted using a Lorentz profile, omitting those parts of the absorption profile contaminated by emission. The radial velocities, shifted to the heliocentric frame, are presented in Table 5. The line centers were then transformed to radial velocities and the resulting curve was fitted in the same manner as the emission-line radial velocities, although γ is not a free parameter here but is defined as the value determined for the $H\alpha$ fit. The data and resulting sine wave fit are shown in Figure 7. The error bars are formal errors from the

TABLE 5
 $H\beta$ ABSORPTION LINE RADIAL VELOCITIES

HJD	V_{rad} (km s^{-1})
2,450,880.8572.....	-103.
2,450,881.6988.....	21.
2,450,881.7458.....	11.
2,450,881.7934.....	178.
2,450,881.8502.....	91.
2,450,882.7582.....	-87.
2,450,882.8044.....	-86.
2,450,882.8547.....	-24.
2,450,882.9010.....	-83.
2,450,882.9412.....	-135.
2,450,883.7348.....	48.
2,450,883.7842.....	76.
2,450,883.8303.....	83.
2,450,883.9156.....	17.

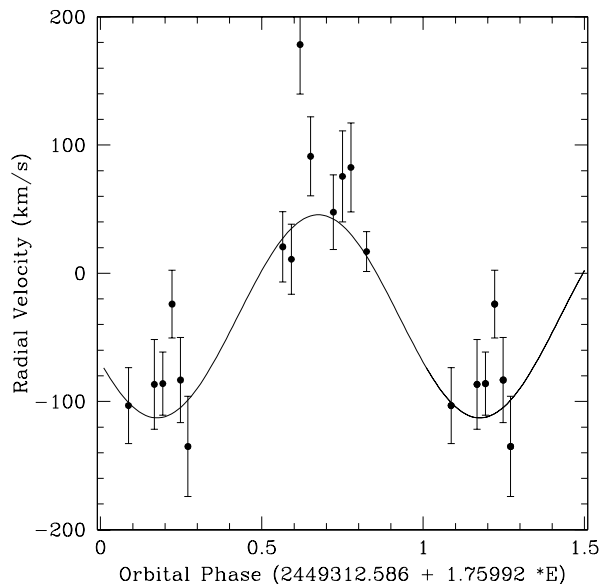


FIG. 7.—Radial velocity curves for the $H\beta$ absorption line constrained to the photometric period.

profile fits. An additional error contribution due to removal of the emission lines is likely present.

3.3. Mass Ratio

Using the radial velocity curves from above, the mass ratio of the system may be estimated. The results arrived at here are approximate for several reasons. First, the absorption lines are not well fitted at our low dispersion because of contamination by emission lines from the secondary. Second, the radial velocity curves found using the emission lines are not truly those of the secondary star because of the emission originating from one hemisphere of the star, not from the entire surface. Therefore we expect the observed amplitude to be smaller than the true amplitude and the derived mass ratio to be an upper limit.

Using the observed K amplitudes of the radial velocity curves for the $H\alpha$ emission ($K_1 \sim 110 \text{ km s}^{-1}$) and $H\beta$ absorption ($K_2 \sim 80 \text{ km s}^{-1}$) curves, we find $q \lesssim 0.7$. Therefore, for a typical white dwarf of $\approx 0.6 M_{\odot}$, $M_2 \lesssim 0.4$. Furthermore, since the light is dominated by the white dwarf in the visual range, the secondary is necessarily a dwarf star.

4. SUMMARY

We conclude that PG 1114+187 is a binary system in which the cool component has an irradiated hemisphere. Minimum light of the system occurs when the heated hemisphere (assumed to be on the secondary) revolves out of view. Taking the source of irradiation to be illumination by a hot primary, this occurs at superior conjunction of the primary or at an emission-line radial velocity of zero (with respect to the center of mass). This produces a 0.25 phase shift of the radial velocity data from the photometric light curve. Similarly, the maximum equivalent width of emission lines occurs when the illuminated face is exposed, producing zero phase shift from the photometric data. Table 6 includes the fitted parameters for the three radial velocity data sets

TABLE 6
SPECTROSCOPIC SINEWAVE FITTED PARAMETERS

Parameter	H α Emission	He I Emission	H β Absorption	EW
γ	-33.6 ± 0.9	-30.3 ± 2.2	-33.6	-4.29 ± 0.03
K	109.9 ± 0.8	92.0 ± 2.4	79.2 ± 9.1	4.19 ± 0.07
ϕ	0.09 ± 0.02	0.01 ± 0.04	0.57 ± 0.18	0.729 ± 0.008

NOTE.— $P = 1.75992$ days and $T_0 = 2,449,312.586$.

and the equivalent-width data. The phasing of the variations in radial velocity, equivalent width, and brightness agrees within errors with the model described above. It is clear that PG 1114+187 is a detached, short-period binary

system consisting of a white dwarf or subdwarf primary and late-type dwarf secondary, leading to the classification of the system as a post-common-envelope and precataclysmic binary.

REFERENCES

- Barstow, M. A., et al. 1995a, *MNRAS*, 272, 531
 Barstow, M. A., Holberg, J. B., Cruise, A. M., & Penny, A. J. 1997, *MNRAS*, 290, 505
 Barstow, M. A., O'Donoghue, D., Kilkenney, D., Burleigh, M. R., & Fleming, T. A. 1995b, *MNRAS*, 273, 711
 Bell, S. A., Pollacco, D. L., & Hilditch, R. W. 1994, *MNRAS*, 270, 449
 Bond, H. E. 2000, in *ASP Conf. Ser. 199, Asymmetrical Planetary Nebulae II: From Origins to Microstructures*, ed. J. H. Kastner, N. Soker, & S. Rappaport (San Francisco: ASP), 115
 Bond, H. E., & Grauer, A. D. 1987, in *IAU Colloq. 95, Second Conference on Faint Blue Stars* (Dordrecht: Kluwer), 221
 Bond, H. E., & Livio, M. 1990, *ApJ*, 355, 568
 Bruch, A. 1999, *AJ*, 117, 3031
 Bruch, A., & Diaz, M. P. 1999, *A&A*, 351, 573
 Bruch, A., & Engel, A. 1994, *A&AS*, 104, 79
 Catalán, M. S., Davey, S. C., Sarna, M. J., Connon-Smith, R., & Wood, J. H. 1994, *MNRAS*, 269, 879
 Chen, A., O'Donoghue, D., Stobie, R. S., Kilkenney, D., Roberts, G., & van Wyk, F. 1995, *MNRAS*, 275, 100
 Delfosse, X., Forveille, T., Beuzit, J.-L., Udry, S., Mayor, M., & Perrier, C. 1999, *A&A*, 344, 897
 Downes, R. A., & Shara, M. M. 1993, *PASP*, 105, 127
 Downes, R. A., Webbink, R. F., & Shara, M. M. 1997, *PASP*, 109, 345
 Ferguson, D. H., & James, T. A. 1994, *ApJS*, 94, 723
 Ferguson, D. H., Liebert, J., Haas, S., Napiwotzki, R., & James, T. A. 1999, *ApJ*, 518, 866
 Fulbright, M. S., Liebert, J., Bergeron, P., & Green, R. 1993, *ApJ*, 406, 240
 Grauer, A. D., & Bond, H. E. 1983, *ApJ*, 271, 259
 Grauer, A. D., Bond, H. E., Ciardullo, R., & Fleming, T. A. 1987, *BAAS*, 19, 643
 Green, R. F., Liebert, J., & Wesemael, F. 1984, *ApJ*, 280, 177
 Green, R. F., Schmidt, M., & Liebert, J. 1986, *ApJS*, 61, 305
 Greenstein, J. L. 1973, *A&A*, 23, 1
 Henden, A. A., & Honeycutt, R. K. 1997, *PASP*, 109, 441
 Honeycutt, R. K. 1992, *PASP*, 104, 435
 Honeycutt, R. K., & Turner, G. W. 1992, in *ASP Conf. Ser. 34, Robotic Telescopes in the 1990s*, ed. A. Filippenko (San Francisco: ASP), 77
 Honeycutt, R. K., Vesper, D., White, J., Turner, G. W., & Adams, B. 1990, in *CCDs in Astronomy II: New Methods and Applications of CCD Technology*, ed. A. G. Philip, D. J. Hayes, & S. J. Adelman (Schenectady: L. Davis), 177
 Horne, J. H., & Baliunas, S. L. 1986, *ApJ*, 302, 757
 Ibanoglu, C., Keskin, V., Akan, M. C., Evren, S., & Tunca, Z. 1994, *A&A*, 281, 811
 Israel, G. L., Stella, L., Angelini, L., White, N. E., Kallman, T. R., Giommi, P., & Treves, A. 1997, *ApJ*, 474, 53
 Kudritzki, R. P., & Simon, K. P. 1978, *A&A*, 70, 653
 Kudritzki, R. P., Simon, K. P., Lynas-Gray, A. E., Kilkenney, D., & Hill, P. W. 1982, *A&A*, 106, 254
 Landolt, A. U., & Drilling, J. S. 1986, *AJ*, 91, 1372
 Lipunova, N. A., & Shugarov, S. Y. 1991, *Inf. Bull. Variable Stars*, 3580, 1
 Livio, M., & Shara, M. M. 1987, *ApJ*, 319, 819
 Lutz, J., Alves, D., et al. (the MACHO Collaboration). 1998, *BAAS*, 192, 5309
 Marilli, E., Frasca, A., Bellina Terra, M., & Catalano, S. 1995, *A&A*, 295, 393
 Marsh, T. R., & Duck, S. R. 1996, *MNRAS*, 278, 565
 Maxted, P. F. L., Marsh, T. R., Moran, C., Dhillon, V. S., & Hilditch, R. W. 1998, *MNRAS*, 300, 1225
 Mendez, R. H., Marino, B. F., Claria, J. J., & van Driel, W. 1985, *Rev. Mexicana Astron. Astrofis.*, 10, 187
 Misselt, K. A., & Shafter, A. W. 1995, *AJ*, 109, 1757
 Moran, C., Maxted, P., Marsh, T. R., Saffer, R. A., & Livio M. 1999, *MNRAS*, 304, 535
 Orosz, J., Wade, R. A., & Harlow, J. J. B. 1997, *AJ*, 114, 317
 Orosz, J. A., Wade, R. A., Harlow, J. J. B., Thorstensen, J. R., Taylor, C. J., & Eracleous, M. 1999, *AJ*, 117, 1598
 Pollacco, D. L., & Bell, S. A. 1994, *MNRAS*, 267, 452
 Saffer, R. A., Livio, M., & Yungelson, L. R. 1998, *ApJ*, 502, 394
 Saffer, R. A., Wade, R. A., Liebert, J., Green, R. F., Sion, E. M., Bechtold, J., Foss, D., & Kidder, K. 1993, *AJ*, 105, 1945
 Sarna, M. J. 1985, *Acta Astron.*, 35, 97
 Scargle, J. D. 1982, *ApJ*, 263, 835
 Schmidt, G. D., Smith, P. S., Harvey, D. A., & Grauer, A. D. 1995, *AJ*, 110, 398
 Schönberner, D. 1978, *A&A*, 70, 451
 Somers, M. W., Lockley, J. J., Naylor, T., & Wood, J. H. 1996, *MNRAS*, 280, 1277
 Stauffer, J. R. 1987, *AJ*, 94, 996
 Taam, R. E., & Spruit, H. C. 1989, *ApJ*, 345, 972
 Thorstensen, J. R., Vennes, S., & Bowyer, S. 1996, *ApJ*, 457, 390
 Tokovinin, A. A. 1997, *A&AS*, 121, 71
 Tylenda, R., Acker, A., Raytchev, B., Stenholm, B., & Gleizes, F. 1991, *A&AS*, 89, 77
 Vennes, S., & Thorstensen, J. R. 1994, *AJ*, 108, 1881
 ———. 1996, *AJ*, 112, 284
 Vennes, S., Thorstensen, J. R., & Polomski, E. F. 1999, *ApJ*, 523, 386
 Walsh, J. R., & Walton, N. A. 1996, *A&A*, 315, 253
 Warner, B. 1995, *Cataclysmic Variable Stars* (Cambridge: Cambridge Univ. Press), 455
 Wood, J. H., Harmer, S., & Lockley, J. J. 1999, *MNRAS*, 304, 335
 Wood, J. H., & Marsh, T. R. 1991, *ApJ*, 381, 551
 Wood, J. H., & Saffer, R. A. 1999, *MNRAS*, 305, 820
 Zwitter, T., & Munari, U. 1994, *A&AS*, 107, 503